

Combined temporal and spatial laser pulse shaping for two-photon excited fluorescence contrast improvement

A. Kussicke, M. Tegtmeier, A. Patas, F. Büchau, K. Heyne, and A. Lindinger*

Institut für Experimentalphysik, Freie Universität Berlin, Arnimallee 14, D-14195 Berlin, Germany

Received: date / Revised version: date

Abstract We report on combined simultaneous temporal and spatial laser pulse shaping by utilizing light polarization properties. Thereto, a setup comprising a temporal pulse shaper, a waveplate, and a spatial shaper was developed and characterized by comparison with simulations. This enables to simultaneously shape one polarization component temporally and spatially while the perpendicular polarization component is modified temporally. The spatially and temporally modulated light fields were recorded and visualized by suitable contour plots, which was particularly demonstrated for cylindrically symmetric pulse profiles. Moreover, temporally and spatially shaped pulses were applied for two-photon excited fluorescence of dyes. These measurements were conducted by scanning third order phase functions for specific spatial pulse components which yields an enhanced contrast difference between fluorescing dyes. The presented temporal and spatial shaping method of ultrashort laser pulses has a high potential for biophotonic applications.

1 Introduction

In recent years laser pulse shaping became an active research field and shaping in the temporal regime was performed for various applications, e.g. control of dissociation [1], isomerization [2], isotope selection [3], biological dynamics [4], and nanooptical fields [5]. Mainly liquid crystal modulators were utilized for tailoring the light fields. Controlling photo-induced molecular processes with temporally shaped pulses has attained considerable success because it enables to drive the induced processes at a maximum yield

* *corresponding author:* lindin@physik.fu-berlin.de

[6,7]. Novel pulse shaping schemes for simultaneous phase, amplitude, and polarization control were developed and a parametric encoding was worked out [8], where the physically intuitive parameters like chirps and polarization states can be controlled. Recently, pulse shaping techniques were employed in life sciences in order to investigate biologically relevant systems. Thereto, laser pulse shaping is particularly applied to multiphoton excitation where intrapulse interference is relevant, which enables to exploit interference effects in multiphoton excited fluorescence spectroscopy [9] and allows for three-dimensional imaging by multiphoton microscopy [10,11]. In particular, these intrapulse interference effects can be employed to selectively excite different molecules via two-photon transitions [12].

It is also possible to manipulate the spatial profile of a laser beam by utilizing spatial light modulators [13,14]. Two dimensional liquid crystal arrays and focussing lenses are used in a setup for spatial pulse shaping. The theoretical concept of spatial pulse shaping evolves around diffraction and is therefore applicable for short laser pulses as well as continuous laser radiation. Modulated spatial beam profiles can be employed e.g. for microstructuring [15] or for high spatial imaging resolution [16,17]. Only a few attempts were made to combine temporal and spatial shaping techniques [18]. However, simultaneous temporal and spatial pulse shaping would be highly desirable for fundamental modification of the entire light field and for concurrently controlling photo-induced processes temporally and spatially. Visualizing doubly shaped pulses is a difficult task and requires an optimization of the data set. It is in some cases possible to represent this initially 4D data set by describing the camera images by a radial intensity function and hence reducing the dimensionality. The radial intensity is combined with the temporal pulse information and mapped onto a contour plot. The contour plot is an effective way to visualize complex spatially and temporally shaped laser profiles.

In this contribution combined temporal and spatial pulse shaping is examined in order to create complex pulse profiles that can then efficiently be used in multiphoton excitation experiments. Specific phase and polarization tailored laser pulses will be presented and scans of antisymmetric phase functions for spatially separated light components are performed to conduct selective two photon induced fluorescence of dyes. The outlined method of spatially and temporally shaped pulses utilizing phase and polarization modulation on multiphoton excitations will lead to novel biophotonic applications in endoscopy and microscopy.

2 Experimental setup

The experimental setup is schematically depicted in Fig. 1. A titanium sapphire laser (FemtSOURCE Compact, Femtolasers) is pumped by a frequency-doubled Nd:YVO₄ laser (Verdi V, Coherent, Inc.). The average power output of the laser system is about 350 mW with a repetition rate of 75 MHz

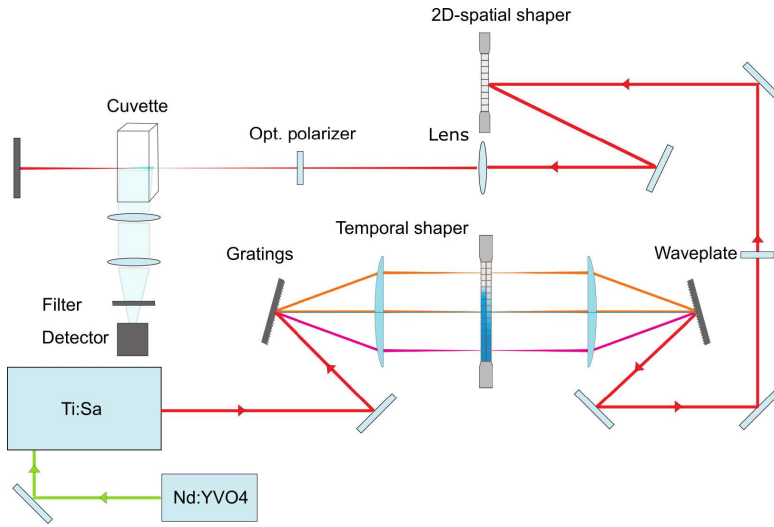


Fig. 1 Experimental setup consisting of a fs-laser (Ti:Sa) and two shapers which are used to control the temporal and spatial properties of the laser pulses. A half wave plate for turning the light polarization is placed between the two shapers. Moreover, a quartz cuvette for fluorescence excitation and devices for light detection are depicted schematically.

and the central wavelength is 802 nm with a bandwidth of 87 nm. The generated pulses are guided through a 4f laser pulse shaper including a liquid crystal light modulator (SLM 640, Cambridge Research Instruments) which is computer controlled. This setup is capable of simultaneously and independently modulating phase and polarization of the laser pulses. The temporally shaped pulses are then directed on the 2D spatial shaper (PLUTO-NIR-015-C, HOLOEYE Photonics AG). The spatial shaper is used to manipulate the spatial profile of the laser pulse. It consists of a 2D array of liquid crystals (1920 x 1080 pixels) and a highly reflective surface which reflects the pulse back. The microdisplay has an active area of 15.36 mm x 8.64 mm. By inserting a focussing lens ($f = 1\text{m}$) after the 2D modulator a 2f setup is realized and the generated spatial laser profile in the focal plane is recorded with a CMOS-camera (DCC1545M, Thorlabs). The CMOS-camera, an autocorrelator (PulseCheck, APE) and a fiber spectrometer (Ocean Optics) function as detectors and are used to visualize the spatial and temporal properties of the laser as well as the characteristics of the investigated dyes. The waveplate, the polarizer and the filter are optional components and are used to optimize the cooperation of both shapers and the signal visualization.

For the fluorescence experiments, the beam is focused after the combined shaper setup into a quartz glass cuvette with the dye solution to be examined. The dyes Rhodamine B (*rhoB*) and Coumarin 102 (*c102*) were

used for two-photon excitations due to their high quantum yields and low fluorescence lifetimes [19,20]. The time between two pulses is roughly 13 ns which is well beyond the fluorescence lifetime of both Coumarin 102 with 6.5 ns [21] and Rhodamine B with 3 ns [19]. The fluorescence maximum of Rhodamine B is roughly at 589 nm and the Coumarin 102 fluorescence peaks at about 470 nm, hence it is well separated for selective detection. The dyes were solvated in ethanol. The laser focus was adjusted to be just behind the glass wall where the beam enters the cell and very close to the glass wall at the side in order to minimize self-absorption and to acquire the maximal signal. The fluorescence light is collected by two lenses after the quartz cell and focused into the detection unit (see Fig. 1). The fluorescence was measured with a spectrometer connected via a fiber. In order to compress the pulses an analytical optimization method, called phase resolved interferometric spectral modulation (PRISM) [22], was implemented which finds the phase required for a transform-limited pulse. The working principle of the optimization is the correlation of a fitness variable with the phase function of the temporal light modulator.

3 Results

3.1 Spatial laser pulse shaping

Spatial laser pulse shaping requires a 2D-modulator in a suitable optical arrangement. We utilize a 2f-setup including the modulator and a lens with 1m focal length placed 1m behind the modulator which leads to a focal plane 1m behind the lens (see Fig. 1). This design is advantageous because it enables to compare the results with simulations employing the spatial 2D-Fourier transformation.

The spatial shaper is programmed to write the phase function on 1000 x 1000 pixels of the totally available 1920 x 1080 pixels. The quadratic active range amounts to 8mm x 8mm and the beam profile has a full width at half maximum of 4.3 ± 0.2 mm which provides a substantial overlap between inscribed phase function and light exposed range. It is important to target the middle of this active area with the Ti:Sa to ensure an optimal spatially shaped laser profile. Adjusting the setup in this regard is achieved in two steps. First, a rough beam alignment is performed by utilizing two mirrors of the setup which generally yields a reasonable quality of the spatially shaped laser profiles. Then, a fine alignment is conducted electronically by shifting the active area (1000 x 1000 pixels) of the shaper on the 2D-Array (1920 x 1080 pixels). During the complete adjustment process the generated spatially shaped laser profile is observed with a CMOS-camera. For alignment purposes an optical vortex phase is written on the spatial shaper which creates a donut shaped spatial profile. Many different phase functions can be used to create a perfect optical vortex as Carvajal et. al have presented recently [23]. The vortex phase has been chosen for the alignment because the quality of the profile can be easily tracked down

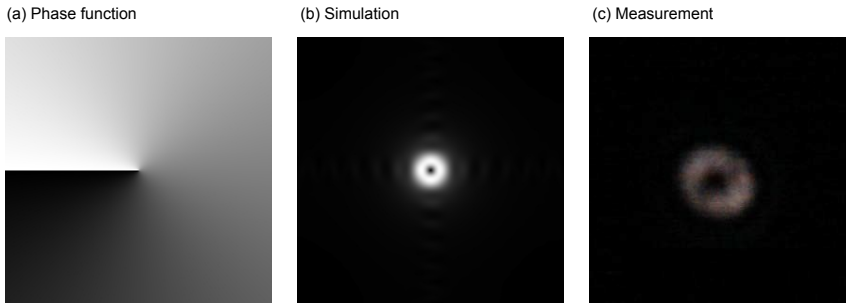


Fig. 2 Donut-shaped spatial profile with the corresponding vortex phase function (a), the theoretically determined far-field image (b), and the experimentally detected image (c). The donut in the experimentally measured image is well visible and symmetric, which indicates a sufficient optimization of the spatial pulse shaper setup.

with the camera and it is simple to generate programatically on the spatial shaper. The phase function, the theoretical expectation of the profile as well as the experimental result are shown in Fig. 2. After the setup has been aligned and a well defined donut shaped profile has been created with the vortex phase, the adjustment is complete. Further experiments can then be performed using different phase functions with more complex spatial profiles.

The linear Zernike polynomials Z_1^1 and Z_1^{-1} are optimal to perform a calibration of the spatial shaper. When written as a phase function on the 2D-array of the shaper they will shift the focus of the laser by a certain distance. Writing Z_1^1 polynomials onto the shaper creates a focus shift on the horizontal axis while Z_1^{-1} polynomials create a shift on the vertical axis. The strength of this focus shift (in units of μm) can be controlled by multiplying the polynomials with a constant. Fig. 3 shows the experimental results of the linear Zernike calibration. To experimentally determine the distance by which the spatial laser profile is shifted a scale can be inserted into the optical pathway. The shift of the focus can then be read of and shows a linear behavior for both Zernike polynomials. In the case of Z_1^1 the data can be fitted with a straight line following the function $(30.7 \pm 0.3)x + 10.8 \pm 26.5$, and for the Zernike polynomial Z_1^{-1} with $(30.5 \pm 0.4)x + 1.6 \pm 37.1$. Being able to control the location of the focus point with a computer can be used to automatically scan the surface of a sample with the laser. Additionally, one can use the linear Zernike polynomials as a phase-offset for the 2D shaper to move more complex spatial profiles in the 2D plane perpendicular to the direction of the optical pathway.

After adjusting the general spatial shaper setup it is possible to begin to write complex phase functions onto the 2D-SLM and compare them with the theoretical expectations. In an initial experiment various Zernike poly-

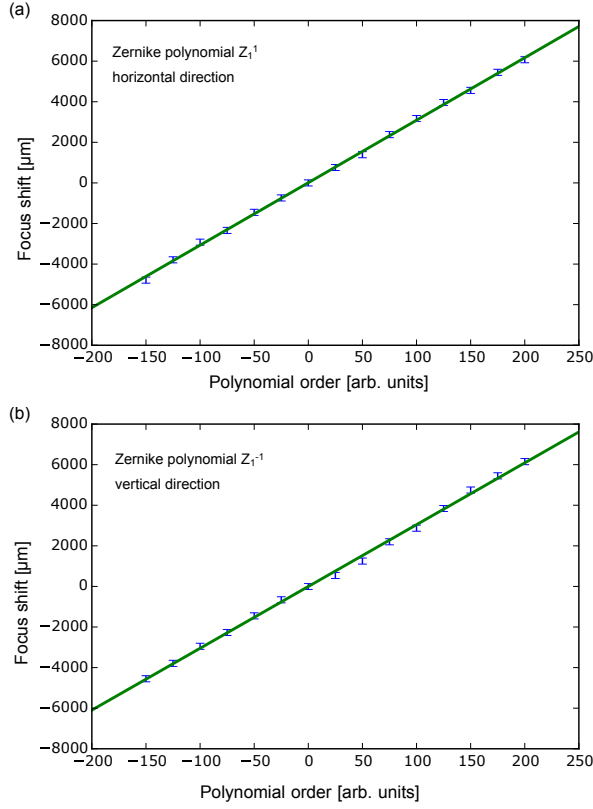


Fig. 3 Results of the linear Zernike polynomial calibration for the two polynomials Z_1^1 (a) and Z_1^{-1} (b). The polynomial orders were chosen from -200 to 250 and a linear behavior of the focus shift can be observed in both cases. The solid lines represent the linear fits. The slopes $30.7 \pm 0.3 \mu\text{m}/\text{order}$ for Z_1^1 and $30.5 \pm 0.4 \mu\text{m}/\text{order}$ for Z_1^{-1} are within one margin of error of each other.

nomials have been used as phase functions to create non-Gaussian spatial laser profiles. The laser profile created by the Zernike phase masks have been observed with a CMOS-camera which was placed at the focus point of the lens behind the spatial shaper. It is necessary to use multiple grey filters (NG1-NG3) to avoid an overexposure of the camera to the laser radiation. Finding the right combination of grey filters is crucial for a good image quality and was performed by observing the Gaussian profile of the laser. The experimentally gained images can be compared to their theoretical counterparts which were simulated by performing a 2D-Fourier transformation with the Zernike phase functions. Fig. 4 shows the experimental and theoretical results for two different Zernike phase functions, namely Z_3^1 and Z_{10}^6 , which were written on the spatial shaper. The theoretical spatial profiles

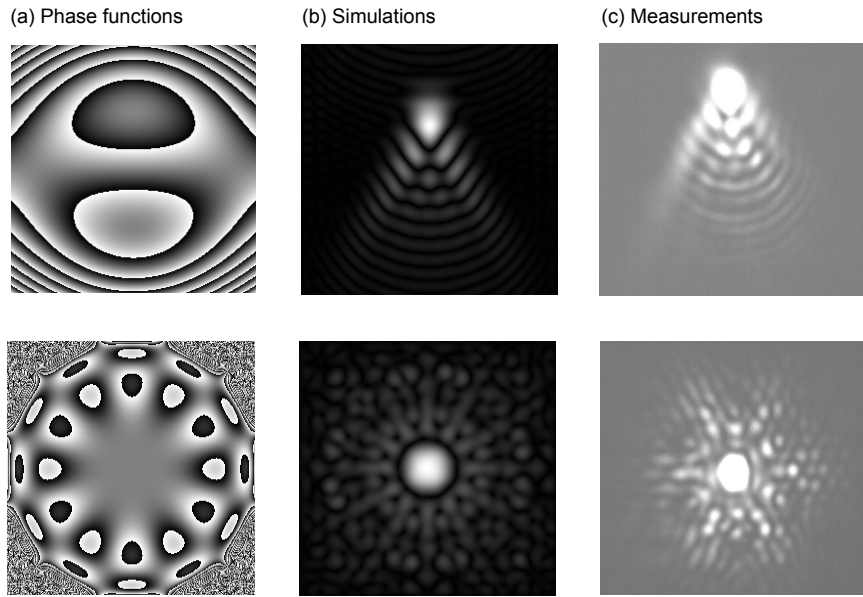


Fig. 4 Spatially shaped laser profiles for different phase functions. The left column (a) displays the corresponding phase functions, the middle column (b) shows the theoretical expectation, and the right column (c) the experimental results measured with a CMOS-camera. The Zernike-polynomials used to generate the spatial profiles are Z_3^1 (top row) and Z_{10}^6 (bottom row)

(Fig. 4 (b)) are highly complex geometric structures with a wide spread intensity distribution. The intensities are normalized on a greyscale and range from 0 (black) to 1 (white). When comparing these theoretical results with the experimentally obtained image (Fig. 4 (c)) it becomes clear that the experimental results very well recreate the theoretical expectations for the phase functions. Due to the limited dynamical range of the CMOS-camera it is however not possible to see all geometric structures of the Zernike phase functions simultaneously, without adjusting the grey filters. A good visualization of this phenomenon is given by the Zernike polynomial Z_{10}^6 where especially the low intensity structures disappear in the experimental image. Removing grey filters reveals the structures. These observations demonstrate a precise spatial control which enables complex photonic applications.

Contrary to the temporal shaper, the spatial shaper is only capable of shaping one polarization direction: The horizontal polarization axis measured relative to the optical bench. The polarization dependence can be shown by writing a vortex phase on the spatial shaper, which generates a donut shaped profile on the horizontal axis. This can be observed with the CMOS-camera, and by inserting a polarizer into the optical pathway one

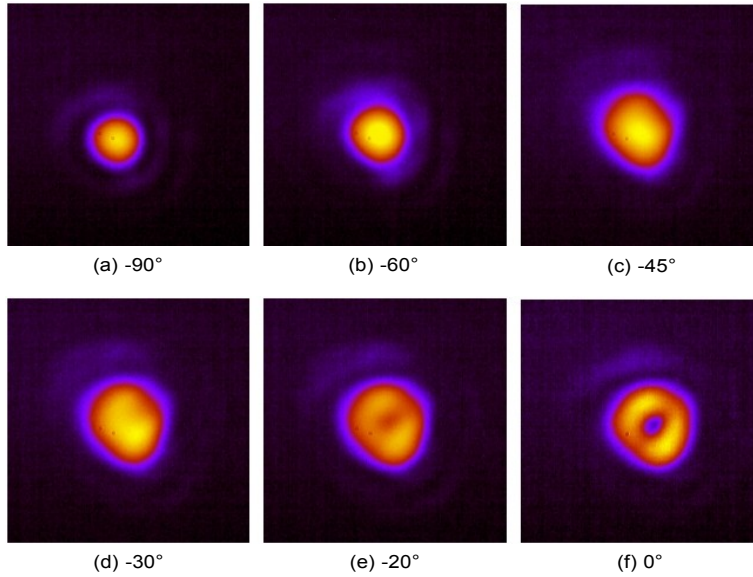


Fig. 5 Polarization component specific spatial pulse shaping. A donut profile is written on the 0° polarization component while a Gaussian profile remains for the -90° polarization component. The different profiles are displayed for the polarizer angles of -90° (a), -60° (b), -45° (c), -30° (d), -20° (e), and 0° (f).

can observe the polarization dependent behavior of the shaper (see Fig. 5). When the polarizer is set to -90° it blocks the horizontally shaped image that was created with the shaper and only the unshaped Gaussian laser profile on the vertical axis is visible. When the polarizer is rotated, the intensity of the spatially shaped image becomes detectable. For increasing polarization angles, the shaped laser profile is visible as an additional donut shaped profile. The intensity of the donut shaped profile, which was measured with the CMOS-camera, increases and gets identical to the original for a polarizer angle of 0° . Therefore, differently shaped profiles can be generated by utilizing the polarization properties which will be exploited to generate spatially and temporally tailored laser pulses by additionally employing a temporal pulse shaper.

3.2 Combined spatial and temporal pulse shaping

After the spatial shaper has been calibrated and optimized the temporal shaper is included which enables to generate spatially and temporally shaped laser pulses. It is mandatory to first pass the temporal shaper and then the spatial shaper because in the reverse case it would not be feasible to perform precise temporal shaping on a spatially expanded laser pulse. As

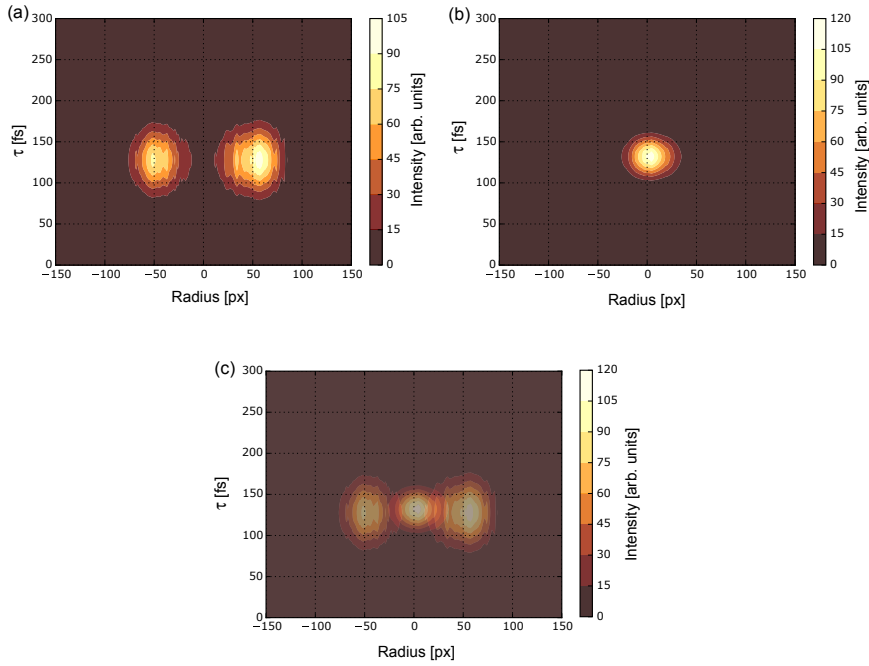


Fig. 6 Combined spatial and temporal pulse shaping visualized as contour plots of radius and autocorrelation delay τ . The pulse shape is first displayed by two individual images which show the horizontal (a) and the vertical polarization axis (b). The combined spatial and temporal pulse intensity is presented in (c). The temporal intensity was measured with an autocorrelator while the spatial intensity was detected with a CMOS-camera. The spatial shaper was used to create a donut profile on the horizontal polarization axis. Moreover, the donut profile exhibits a temporal broadening due to a linear chirp applied on the same polarization component by the temporal pulse shaper. Therefore, the vertical delay image widths of the donut profile is larger than that of the central profile. This proves simultaneous spatial and temporal laser pulse shaping.

it was mentioned in the previous section it is only possible to manipulate the horizontal polarization axis with the spatial shaper.

The temporal shaper on the other hand manipulates the spectral phase on two polarization axes which are rotated by 45° to the optical bench. A $\lambda/2$ -waveplate is inserted into the optical pathway and rotates the temporally shaped polarization axes of the pulse into the vertical and horizontal direction, hence they are projected on the vertical and horizontal axes of the 2D shaper in order to enable different spatial shapes of these components. With this configuration of the experimental setup, the horizontal polarization component can be spatially shaped while the vertical polarization component will remain as a Gaussian-profile for all measurements. Imaging

spatially and temporally shaped pulses is difficult since it is effectively a 4D problem: Each polarization direction has its own 2D spatial intensity profile as well as an independent time behaviour. To visualize the complete laser profile, including both spatial and temporal information of the pulse, it is therefore necessary to reduce the 2D spatial profile to a 1D image. This problem can be addressed for most radial symmetric profiles without losing crucial information by plotting the image intensity against the radius of the object instead of a 2D grid. The spatial image intensity for each radial value is then multiplied with the autocorrelation intensity for each autocorrelation delay of the pulse. The result can be visualized in a contour plot which simultaneously shows the spatial intensity and the temporal autocorrelation intensity of the pulse.

Fig. 6 shows a temporally and spatially shaped laser pulse profile as contour plots of radius and autocorrelation delay τ . The spatial profile of the laser was manipulated with the 2D-LCM using a vortex phase. This creates a donut image on the horizontal polarization axis of the laser pulse. The spectral phase of the pulse was manipulated on both polarization axes. To create a transform-limited pulse, the spectral phase found by the PRISM algorithm was used as an offset phase for the temporal shaper. The spectral phase on the horizontal axis was then additionally shaped by applying a positive linear chirp of 1000 fs^2 to create a broader pulse in one polarization component. The resulting pulse shape can technically be visualized in a single image. The image separation into horizontal and vertical polarization components has been performed exclusively to enhance the visibility of the complete laser profile. It can be the case that the two polarization dependant profiles have overlapping components in time or space which aggravates the visualization of the complete profile. Then it is therefore mandatory to present the pulse shapes of each polarization axis individually. The new developed pulse presentation visualizes the pulse properties and provides a proof for simultaneous spatial and temporal laser pulse shaping.

3.3 Contrast enhancement by spatial and temporal pulse shaping on dyes

The previously presented experimental techniques and procedures can be combined to perform multiphoton excitations of dyes with spatially and temporally shaped laser pulses in order to improve the contrast. The experimental advantages of using simultaneously spatially and temporally shaped pulses, emitted by a single light source, can be immense in fluorescence spectroscopy. E.g. exciting multiple samples at once, creating a STED-microscope with a single femtosecond laser, or increasing the contrast for imaging. This section will therefore be dedicated to generate experimental data to show that simultaneously spatially and temporally shaped laser pulses can be used effectively in fluorescence experiments.

Two spatially separated Gaussian profiles were generated in the focal plane by spatial pulse modulation which enables to simultaneously detect

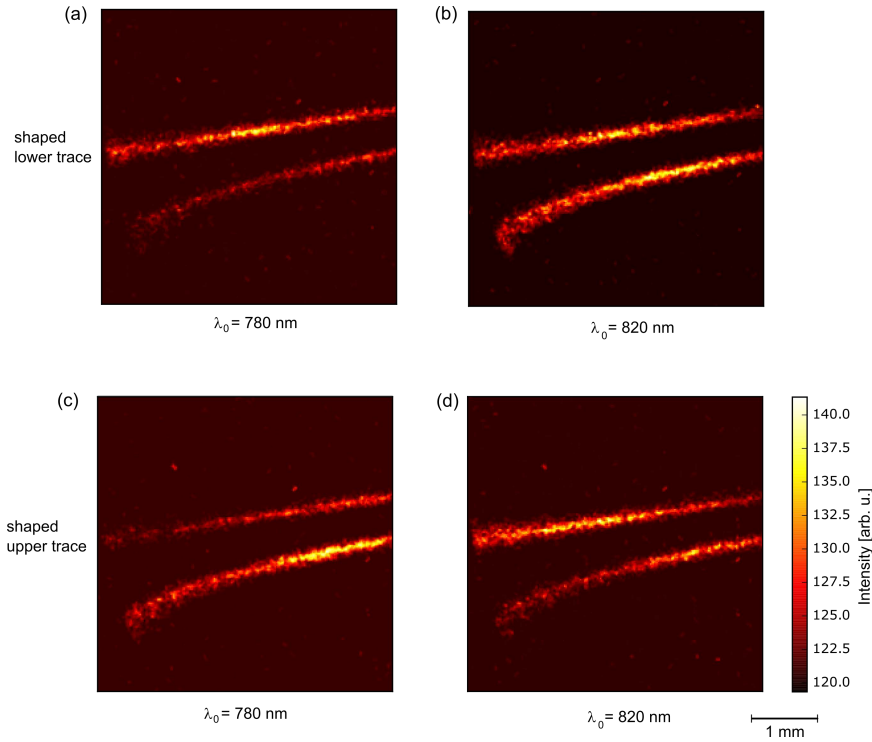


Fig. 7 Images of the fluorescence intensities of Rhodamine B in a cuvette induced by spatially separated pulse polarization components. (a) Image for the unshaped vertical polarization component (upper trace) and the third order phase shaped horizontal component for $\lambda_0 = 780$ nm (lower trace). (b) Corresponding figure for $\lambda_0 = 820$ nm. (c) Image for the unshaped horizontal polarization component (lower trace) and the third order phase shaped vertical component for $\lambda_0 = 780$ nm (upper trace). (d) Corresponding figure for $\lambda_0 = 820$ nm. The spatially separated horizontal components show differing fluorescence intensities. This demonstrates simultaneous spatial and temporal pulse shaping in two photon excitation fluorescence.

their specific fluorescence with a camera. For improved focussing a lense with 100 mm focal length was additionally inserted in front of the cuvette. One Gaussian profile corresponds to the horizontal and the other one to the vertical polarization component. To determine the contrast of Coumarin 102 and Rhodamine B a third order phase scan was performed on the LCM-array of the temporal shaper relating to the horizontally polarized spatial Gaussian profile. The antisymmetric third order phase has the advantage to yield a sharp maximum of the two-photon field [12]. By shifting the position of the antisymmetric function on the temporal shaper the turning point of the function and hence the sharp maximum is shifted to different

wavelengths [24]. This enables to scan the spectrum of the Ti:Sa laser with the antisymmetric phase function for the individual dyes. The position of the turning point (λ_0) of the antisymmetric function is shifted in steps of one shaper-pixel at a time (a pixel corresponds to 1.305 nm) and the fluorescence intensity is recorded as a function of the central position of the antisymmetric phase function. The second LCM-array was left unused for the duration of the scan i.e. no additional phase functions were applied to the array. The fluorescence intensity is measured with the camera, as a function of λ_0 , for a specific polarization direction of the laser pulse. Fluorescence intensity images of Rhodamine B in a cuvette excited by spatially separated pulse polarization components were conducted with the camera directed perpendicular to the beam axis (see Fig. 7). Images were taken for the unshaped vertical polarization component (upper traces) and the third order phase shaped horizontal component (lower traces) for $\lambda_0 = 780$ nm and $\lambda_0 = 820$ nm, respectively, and for the unshaped horizontal polarization component (lower traces) and the third order phase shaped vertical component (upper traces). The images display spatial shaping of different polarization components and the phase shaped traces show low fluorescence intensities for $\lambda_0 = 780$ nm and high intensities for $\lambda_0 = 820$ nm, respectively. Thus, each spatially separated trace can be individually temporally shaped. These figures demonstrate combined spatial and temporal pulse shaping for a two photon excitation fluorescence application.

Since the two polarization directions are separated in space due to the applied linear Zernike polynomial, one can simply integrate over the two fluorescence signals individually. This was performed in a separate measurement with a camera located perpendicular to the beam direction in order to remove the signal from the front surface of the cuvette. For the integration a software was programmed that slices the camera images in half and then sums over all illuminated pixels of the CMOS-sensor. The cutting process is required to separate the two fluorescence beams of the camera image from each other before the integration. To maximize the signal to noise ratio, 51 images have been taken in total for each value of λ_0 . The images have then been averaged and were finally integrated to determine the fluorescence intensities. The phase scans were performed for both dyes individually to simplify the experimental procedure. The results of the third order phase scan are shown in Fig. 8 (a) for Coumarin 102 and in Fig. 8 (b) for Rhodamine B. The results of the Coumarin 102 scan show a clear maximum of the fluorescence intensity at $\lambda_0 = 812$ nm for the spatially and temporally shaped pulse component (blue line). For the unshaped component of the pulse (green line) there is no intensity change visible during the scan.

A similar behavior is observed for the Rhodamine B scan. The intensity maximum is clearly visible for the temporally and spatially shaped pulse component and it is located at $\lambda_0=825$ nm. The unshaped pulse component on the vertical polarization axis is unaffected by the third order phase scan that was performed on the horizontal polarization axis with the temporal

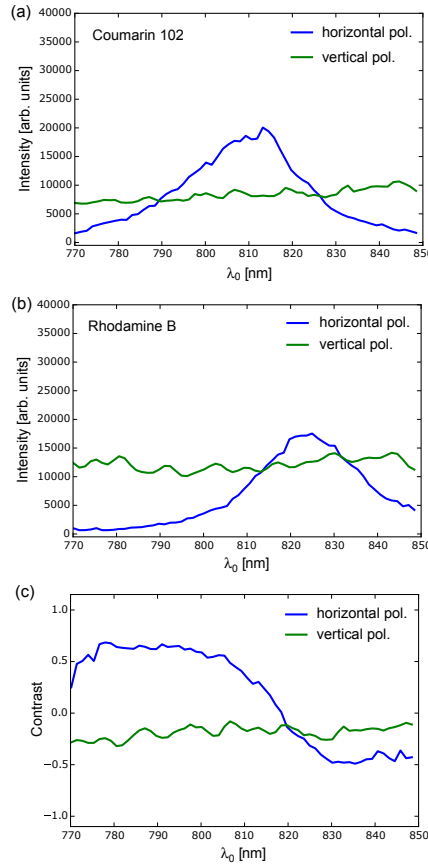


Fig. 8 (a) Fluorescence intensity of Coumarin 102 for a third order phase scan on the horizontal pulse polarization component (blue) which is also spatially shaped with the 2D-shaper. The intensity on the unshaped vertical polarization component (green) is constant during the third order phase scan. (b) Corresponding measurement for Rhodamine B. (c) Contrasts between Coumarin 102 and Rhodamine B for the two polarization directions. A clear contrast difference is obtained for the horizontal polarization component.

shaper. The slightly lower intensity of the vertical component compared to the maxima of the horizontal component can be explained by the reduced light intensity of the vertical component due to polarization dependent reflection of the optical components. The experimental data clearly indicate that temporally and spatially shaped laser pulses can be generated with a desired pulse profile which can effectively be used for multiphotonic excitations of dyes in fluorescence experiments.

The data obtained from the phase scans are used to determine the contrasts of the two dyes with $C = (I_{C102} - I_{Rhob}) / (I_{C102} + I_{Rhob})$. The con-

trasts are shown in Fig. 8 (c) for the wavelength region of λ_0 present in the spectrum of the laser. The contrast calculation is based on the third order phase scan that was carried out on the horizontal LCM-array of the temporal shaper. The contrast of the horizontal component is positive for $\lambda_0 < 820$ nm and negative for $\lambda_0 > 820$ nm and exhibits a total contrast difference of about 1.1, which can be regarded as a very good separation. The data clearly demonstrate that the contrast between two two-photon dyes can be determined and improved by using simultaneously spatially and temporally shaped laser pulses.

4 Conclusions

In a first experimental step the 2D-spatial light modulator was calibrated. After adjusting the optical pathway as well as the software it was possible to generate spatially shaped laser pulses. These spatial profiles were created by writing two dimensional phase functions onto the shaper array such as a vortex phase and Zernike polynomials. The generated two dimensional intensity distributions were then imaged with a photosensitive CMOS-camera. They matched their theoretically calculated counter parts well and even highly complex profiles could be produced without losing image quality. It is however crucial for the experimental procedure that the laser illuminates the active surface of the shaper in the center otherwise the desired pulse profile can show irregularities. Similiar problems arise if the incoming laser pulse is not of perfect gaussian shape. The temporal and spatial shapers were afterwards used simultaneously to create spatially and temporally shaped laser pulses. This was realized by modifying the laser fields such that one polarization component was tailored simultaneously temporally and spatially, whereas its perpendicular polarization component was shaped temporally. Visualizing doubly shaped pulses is a difficult task and required an optimization of the data set. It is possible to portray this initial 4D data set by describing the camera images by a radial intensity function instead of a 3D intensity profile. The radial intensity is combined with the temporal pulse information and mapped onto a contour plot. Contour plots are well suited to visualize complex spatially and temporally shaped pulses.

Following, the experimental setup was adjusted to perform fluorescence experiments with spatially and temporally shaped laser pulses. It was shown that temporally and spatially tailored pulses can be controlled and that they can effectively be used in fluorescence experiments. A pulse profile was generated that seperated the horizontal and vertical polarized pulse components in space. Using this spatial profile the contrast of the two dyes Coumarin 102 and Rhodamine B was determined based on a third order phase scan that was carried out exclusively on the horizontal polarization axis. The fluorescence measurements showed that the pulse was modulated in space and time since only the fluorescence intensity on the horizontally shaped pulse component changed during the third order scan. The calculated contrast

change was significant during the scan. Both dyes have notably different fluorescence signals for phase scans of the central frequencies which is the main reason for the strong contrast change.

The experimental data clearly shows that laser pulses can be controlled effectively in space and time simultaneously, with the limitation that one polarization component could not be modulated spatially. Temporally and spatially shaped pulses can be applicable in many modern experiments such as STED microscopy or medical investigations. A STED microscope for example generally requires two laser beams with different spatial profiles. One laser is used for the excitation of a sample while the second one initiates stimulated emission in a surrounding area. In order to achieve different wavelengths for the exciting and the de-exciting beam third order phase functions with different antisymmetry points could be written on the different arrays of the temporal modulator. This enables a two-photon de-excitation transition at a differing wavelength than the exciting beam. Due to long life times of the excited states of the molecules it is moreover advantageous to separate the exciting and deexciting pulses in time [16]. A possible time-dependent frequency change of the deexcitation process could even be adapted by temporally chirping the pulse component. All of the described experimental inconveniences can theoretically be addressed by using spatially and temporally shaped pulses generated by a single femtosecond laser. The current experimental setup is therefore well suited for further research in STED microscopy. Apart from direct physical applications for simultaneously spatially and temporally shaped pulses there is also demand in medical research. In recent cancer diagnostics, fluorescence dyes and proteins have been utilized to mark and visualize tumor cells in vivo [25]. It is often a problem to image the cancer cells without significant background noise coming from surrounding tissue [26]. The high selectivity of two photon processes combined with the variety of different available spatial laser profiles can be a great addition for optimal cancer cell imaging.

5 Acknowledgement

The Klaus Tschira Foundation (KTS) is acknowledged for financial support (project 00.314.2017).

References

1. A. Assion, T. Baumert, M. Bergt, T. Brixner, B. Kiefer, V. Seyfried, M. Strehle, G. Gerber, *Science* **282** (1998) 919-922.
2. G. Vogt, G. Krampert, P. Niklaus, P. Nuernberger, G. Gerber, *Phys. Rev. Lett.* **94** (2005) 068305.
3. A. Lindinger, C. Lupulescu, M. Plewicky, F. Vetter, A. Merli, S. M. Weber, L. Wöste, *Phys. Rev. Lett.* **93** (2004) 033001.
4. W. Wohlleben, T. Buckup, J. L. Herek, M. Motzkus, *ChemPhysChem* **6** (2005) 850-857.

5. M. Aeschlimann, M. Bauer, D. Bayer, T. Brixner, F. J. Garcia de Abajo, W. Pfeiffer, M. Rohmer, C. Spindler, F. Steeb, *Nature* **446** (2007) 301-304.
6. R. S. Judson, H. Rabitz, *Phys. Rev. Lett.* **68** (1992) 1500-1503.
7. T. Brixner, G. Gerber, *ChemPhysChem* **4** (2003) 418-438.
8. F. Weise, A. Lindinger, *Appl. Phys. B* **101** (2010) 79-91.
9. K. A. Walowicz, I. Pastirk, V. V. Lozovoy, M. Dantus, *Phys. Chem. A* **106** (2002) 9369-9373.
10. W. Denk, J. H. Strickler, W. W. Webb, *Science* **248** (1990) 73-76.
11. S. Perry, R. Burke, E. Brown, *Ann. Biomed. Eng.* **40** (2012) 277.
12. V. V. Lozovoy, I. Pastirk, K. A. Walowicz, M. Dantus, *J. Chem. Phys.* **118** (2002) 3187-3196.
13. N. Sanner, N. Huot, E. Audouard, C. Larat, J.-P. Huignard, *Opt. Lett.* **30** (2005) 1479-1481.
14. C. Maurer, A. Jesacher, S. Bernet, M. Ritsch-Marte, *Laser Photonics Rev.* **5** (2011) 81-101.
15. N. Sanner, N. Huot, E. Audouard, C. Larat, J.-P. Huignard, *Opt. Lasers Eng.* **45** (2007) 737-741.
16. S. Hell, J. Wichmann, *Opt. Lett.* **19** (1994) 780-782.
17. G. Moneron, S. Hell, *Opt. Exp.* **17** (2009) 14567-14573.
18. T. Feurer, J. C. Vaughan, R. M. Koehl, K. A. Nelson, *Opt. Lett.* **27** (2002) 652-654.
19. M. J. Snare, F. E. Treloar, K. P. Ghiggino, P. J. Thistlethwaite, *J. Photochem.* **18** (1982) 335-346.
20. R. F. Kubin, A. N. Fletcher, *J. Luminescence* **27** (1982) 455-462.
21. J. H. Richardson, L. L. Steinmetz, S. B. Deutscher, W. A. Bookless, W. L. Schmelzinger, *J. Phys. Chem.* **33** (1978) 15921593.
22. T. Wu, J. Tang, B. Hajj, M. Cui, *Opt. Express* **19** (2011) 12961.
23. N. A. Carvajal, C. H. Acevedo, Y. T. Moreno, *Int. J. Opt.* **2017** (2017) 6852019.
24. A. Patas, G. Achazi, N. Hermes, M. Pawowska, A. Lindinger, *Applied Physics B: Lasers and Optics* **112** (2013) 579-586.
25. G. M. van Dam and G. Themelis, L. M. A. Crane, N. J. Harlaar, R. G. Pleijhuis, W. Kelder, A. Sarantopoulos, J. S. de Jong, H. J. G. Arts, A. G. J. van der Zee, J. Bart, P. S. Low, V. Ntziachristos, *Nat. Med.* **17** (2011) 1315.
26. Y. Urano, D. Asanuma, Y. Hama, Y. Koyama, T. Barrett, M. Kamiya, T. Nagano, T. Watanabe, A. Hasegawa, P. L. Choyke, H. Kobayashi, *Nat. Med.* **15** (2009) 104.